第34卷 第7期 焊 接 学 报 Vol. 34 No. 7
2013年7月 TRANSACTIONS OF THE CHINA WELDING INSTITUTION July 2013

三维搅拌摩擦焊接传热与塑性流动分析模型

冯天涛， 张晓辉
（山东农业大学 山东省园艺机械与装备重点实验室，泰安 271018）

冯天涛

摘 要： 为研究搅拌摩擦焊接过程热流相互作用下的温度场、速度场和粘度场，将材料看成是层流、粘性、非牛顿流体，基于流体力学理论，建立了搅拌摩擦焊接过程的三维热流分析模型. 给出了焊接过程热输入与搅拌头的旋转频率、工件运动速度、搅拌头尺寸及材料发生屈服时的剪应力的数学关系式，并将其作为热边界条件加入到了模型中. 结果表明，搅拌头前部温度低于后部，温度梯度前部大于后部；受搅拌头周围材料流动的影响，接近搅拌针的区域，后退侧温度高于前进侧；材料上部速度、粘度受轴肩影响较大，下部主要受搅拌针影响；计算得到的热力影响区与试验结果有较好的对应关系.

关键词： 搅拌摩擦焊；流体力学；热流耦合；剪应力
中图分类号： TG453 **文献标识码：** A **文章编号：** 0253－360X(2013)07－0105－04

0 序 言

搅拌摩擦焊（friction stir welding，FSW）是一种固相连接新技术，与传统焊接方法相比，具有很多优点，可以用来焊接很多过去认为难以焊接的金属[1,2]. 近年来国内外学者对其产热机理和塑性流动进行了大量的研究，大多数将两者割裂开来，计算产热时不考虑材料的流动，而计算塑性流动时又对产热模型进行大量的简化.

Song 等人[3]建立了三维 FSW 过程的热模型，认为焊接过程中的热量由两部分组成：轴肩与工件的摩擦产热和搅拌针周围材料的剪切变形产热，但没有考虑搅拌头周围材料流动的影响. Schmidt 等人[4]认为热量来自于搅拌头和工件在接触界面处的摩擦产热和塑性变形产热，考虑了搅拌头周围材料流动的影响，但计算时需要给出搅拌头轴向压力、摩擦系数及接触状态系数. Schmidt 等人[5]还认为被焊材料随温度变化的屈服应力是影响产热的主要因素. 李红克等人[6]建立了热量自适应的搅拌摩擦焊接模型，认为热量随温度、材料性能而改变. 赵衍华等人[7]利用 FLUENT 软件建立了 FSW 过程的数值分析模型，认为热量完全由粘性耗散产生.

为了分析热流相互作用下的温度场、速度场和粘度场，文中利用 FLUENT 软件，建立了基于流体力学的 FSW 过程三维热流分析模型，焊接过程中的热输入与搅拌头旋转频率、焊接速度、搅拌头尺寸及材料发生屈服时的剪应力有关，考虑了搅拌头周围材料流动的影响.

收稿日期： 2012－05－29

1 模型的建立

文中将 FSW 过程中的材料看作是绕过旋转圆柱体的层流、粘性、非牛顿流体，计算时仅考虑准稳态时的热流耦合情况.

1.1 产热模型

FSW 过程中的焊接热输入来自于搅拌头与工件接触区域的摩擦产热和塑性变形产热，当焊接过程达到准稳态时，接触区域的任一点的摩擦剪切应力等于材料发生塑性变形时的剪切应力[5]. 分析时轴肩、搅拌针侧面和底面与工件在接触区域所产生的热量均予以考虑.

轴肩与工件在接触区域由于摩擦和塑性变形而产生的热量可表示为

$$q_{zj}=C_f\left(\omega\sqrt{x^2+z^2}-v_g\frac{z}{\sqrt{x^2+z^2}}\right)\tau_{yield} \quad (1)$$

式中：C_f 为搅拌头与工件在接触区域产生的热量传入到工件的比例，文中取为 0.85；ω 为搅拌头的旋转频率；v_g 为工件运动速度（焊接速度与其大小相等，方向相反）；x，z 为搅拌头与工件接触区域的坐标. 搅拌针侧面与工件在接触区域由于摩擦和塑性变形而产生的热输入可表示为

$$q_{zc}=C_f\left(\omega r-v_g\frac{z}{r}\right)\tau_{yield} \quad (2)$$

式中: r 为搅拌针的半径; τ_{yield} 为材料发生屈服时的最大剪切应力. 搅拌针底面与工件在接触区域由于摩擦和塑性变形而产生的热输入与式(1)相同.

工件与搅拌头的接触条件认为是部分滑移粘着状态[4],与搅拌头接触的材料随搅拌头一起旋转,旋转频率均取为 0.65ω. τ_{yield} 与屈服强度的关系为

$$\tau_{\text{yield}} = R_{\text{eL}}/\sqrt{3} \tag{3}$$

而材料的屈服强度随温度的上升而减小[5],当温度达到一定值后,屈服强度减少为 0,搅拌头与工件的接触区域就不再产生热量,温度就不再上升.

1.2 主控方程

在 FSW 过程中,塑性材料被看作是流体,流体连续流动应遵循的基本方程为质量守恒方程、动量守恒方程和能量守恒方程.

质量守恒方程表达式为

$$\frac{\partial u}{\partial x}+\frac{\partial v}{\partial y}+\frac{\partial w}{\partial z}=0 \tag{4}$$

式中: u, v, w 代表 3 个方向上的流体速度分量.

动量守恒方程采用 Navier-Stokes 形式写为

$$\rho\frac{\mathrm{d}V}{\mathrm{d}t}=-\nabla p-\nabla\tau+\rho G \tag{5}$$

式中: ρ 为平均密度; V 为流体速度,其分量为 u, v, w; p 为静态压力; G 为重力; τ 为剪切应力.

$$\tau=\eta(T,\bar{\varepsilon})\left(\frac{\partial u}{\partial x}+\frac{\partial v}{\partial y}+\frac{\partial w}{\partial z}\right) \tag{6}$$

式中: η 为粘度; T 为温度; $\bar{\varepsilon}$ 为平均应变率.

稳态能量守恒公式为

$$\rho c_{\text{p}}\left(u\frac{\partial T}{\partial x}+v\frac{\partial T}{\partial y}+w\frac{\partial T}{\partial z}\right)=$$
$$\frac{\partial}{\partial x}\left(\lambda\frac{\partial T}{\partial x}\right)+\frac{\partial}{\partial y}\left(\lambda\frac{\partial T}{\partial y}\right)+\frac{\partial}{\partial z}\left(\lambda\frac{\partial T}{\partial z}\right) \tag{7}$$

式中: c_{p} 为比热容; λ 为热导率.

式(4),式(5),式(7)组成一个非线性、全耦合的控制方程,用来描述稳态、非牛顿、不可压、忽略重力的流体流动.

1.3 计算区域与边界条件

FSW 过程中搅拌头垂直于工件,轴肩是一个平面,直径为 26 mm; 搅拌针为光滑圆柱体,直径为 5.9 mm,长度为 5.6 mm. 搅拌头作逆时针旋转运动,旋转频率为 600 r/min,工件自左向右沿 x 正方向匀速运动,速度为 90 mm/min. 为节省计算时间,只取工件的一部分进行计算,计算区域为一圆柱形区域, x 方向为 52 mm,即两倍的轴肩直径, z 方向为 50 mm, y 方向为板厚 6.3 mm,如图 1 所示.

轴肩、搅拌针侧面及底面为热输入边界,其热流量见 1.1 节. 上表面、下表面、前进侧和后退侧的边界均设置为移动墙,速度与工件运动速度相同. 流体入口边界设置为速度入口边界条件,且速度等于工件运动速度,流体出口边界设置为压力出口边界条件. 上表面暴露于空气中,是一种热对流边界,热对流系数取为 50 W/(m^2·K); 下表面与垫板接触,热传导系数取为 500 W/(m^2·K); 前进侧和后退侧部分与空气接触,部分与夹具接触,设置其热传导对流系数取为 200 W/(m^2·K). 初始温度设为 300 K.

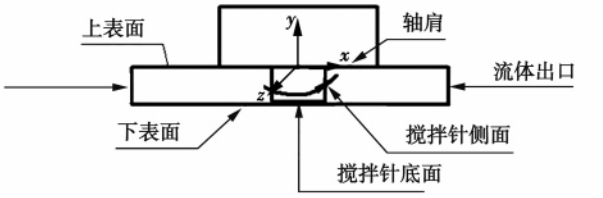

图 1 计算区域示意图

Fig. 1 Schematic computational zone

1.4 材料物性

文中分析选用 6061 铝合金. 粘度在流场计算中是一个非常重要的参数,它与温度和平均应变率有关. 根据文献[8],材料的粘度可以用下式表示为

$$\eta(T,\bar{\varepsilon})=\frac{1}{3\bar{\varepsilon}\alpha}\ln\left(\left(\frac{Z(T,\bar{\varepsilon})}{A}\right)^{\frac{1}{n}}+\left(1+\left(\frac{Z(T,\bar{\varepsilon})}{A}\right)^{\frac{2}{n}}\right)^{\frac{1}{2}}\right) \tag{8}$$

$$Z(T,\bar{\varepsilon})=\bar{\varepsilon}\exp\left(\frac{Q}{RT}\right) \tag{9}$$

式中: α, $\ln A$, n 为与材料有关的常数,文献[8]给出了 6061 铝合金对应的常数值,其中 $\alpha=0.045/\text{MPa}$; $\ln A=19.3/\text{s}$; $Q=145\ 000$ J/mol; $n=3.55$,通用气体常数 $R=8.314$ J/(mol·K). 根据文献[9],忽略密度随温度的变化,密度取为 2 700 kg/m^3,将 6061 铝合金的热导率 λ、比热容 c_{p} 和屈服强度 R_{eL} 随温度变化的数据进行拟合,即

$$\lambda=25.22+0.397\,8T \tag{10}$$

$$c_{\text{p}}=929.3-0.627T \tag{11}$$

$$R_{\text{eL}}=\begin{cases}182.16+0.715\,44T-0.001\,34T^2 & T\leqslant 477\\ 3\,671.57-14.29T+0.018\,7T^2 & T\leqslant 855\end{cases} \tag{12}$$

2 模拟结果及分析

采用隐式、线性、分离解算器进行计算并对网格进行离散. 在求解过程中,应用标准离散方程计算压力,应用二阶逆风方程计算动量方程,应用一阶逆风方程计算能量方程.

2.1　热量分布

FSW 过程中轴肩产热的热量大约占总热量的 80% ~90% [9],文中计算结果表明轴肩产生的热量为 1.455 kW,搅拌针侧面产生的热量为 0.183 kW,搅拌针底面产生的热量为 0.027 kW,轴肩产热约占总热量的 87%.

2.2　温度场

经搅拌头的轴线将计算的温度场沿纵向和横向切片如图 2 和图 3 所示,工件上表面的温度如图 4 所示. 计算表明峰值温度为 759 K,约为 6061 铝合金液相线温度的 89%.

图 2　*xy* 平面($z=0$) 的温度场分布

Fig. 2　Temperature field of *xy* plane ($z=0$)

图 3　*yz* 平面($x=0$) 的温度场分布

Fig. 3　Temperature field of *yz* plane ($x=0$)

由图 2 可知,搅拌头前部($x<0$) 的温度要低于后部($x>0$) ,前部的温度梯度大于后部. 前者是由于材料绕旋转的搅拌针由前部流向后部,而后者是因为搅拌头前方材料温度低,不断进入焊接过程被加热,后部材料处于焊后状态,仅通过热传导和对流向外散热. 由图 3 可知焊缝前进侧($z<0$) 的温度梯度小于后退侧($z>0$) ,这是由于焊接速度的影响使前进侧产热的热量较多. 但从图 4 可以看出,在接近搅拌针的区域,后退侧的温度要高于前进侧,这是由于在该区域内,材料发生较大塑性变形,从前进侧流经后退侧,部分热量在材料流动的过程中以热对流的方式将热量传递给了后退侧的材料. 而采用热电偶测量温度时热电偶安放在远离搅拌针的区域,不受此影响,前进侧温度要稍高于后退侧.

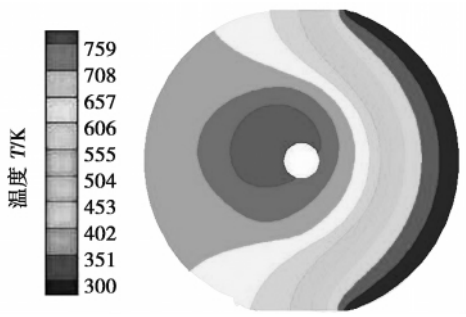

图 4　*xz* 平面($y=0$) 的温度场分布

Fig. 4　Temperature field of *xz* plane ($y=0$)

2.3　速度场

垂直于搅拌头的轴线将计算的速度场沿横向切片如图 5 和图 6 所示.

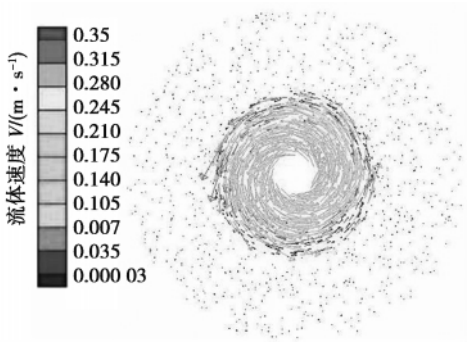

图 5　$y=-1$ 平面的速度场分布

Fig. 5　Velocity field of *xz* plane $y=-1$

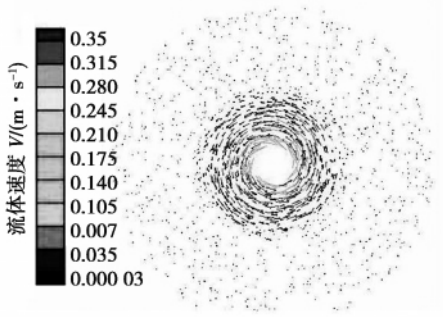

图 6　$y=-2$ 平面的速度场分布

Fig. 6　Velocity field of *xz* plane $y=-2$

从图 5 和图 6 中可以看出,靠近轴肩,材料流动速度变大,易流动范围变大,远离轴肩则相反; 同一平面上,靠近搅拌针,速度增大,反之减小. 工件上部受轴肩影响较大,下部主要受搅拌针影响.

2.4　粘度场

搅拌针周围粘度分布范围为 4.24×10^4 ~ 5×10^6 kg/(m·s) ,如图 7 所示. 当粘度超过 5×10^6

kg/(m·s)时,材料不发生明显的塑性流动[9],因而将上述计算范围对应于接头的热力影响区,在工件上表面与轴肩尺寸基本一致,远离上表面,轴肩影响变小,此范围也变小. 图 8 为采用相同工艺参数进行搅拌摩擦焊接得到的接头横截面[9],图 8 中实线标出的是该试验条件下的热力影响区,对比图 7 可以看出,二者有较好的对应关系.

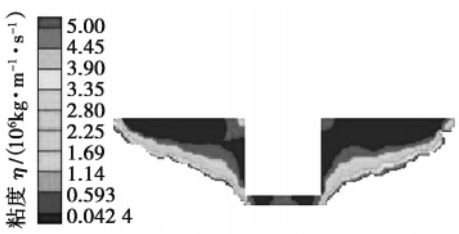

图 7 *xy* 平面的粘度分布

Fig. 7 Viscosity field of *xy* plane

图 8 搅拌摩擦焊接接头横截面

Fig. 8 Cross section of friction stir weld seam

3 结 论

(1) 基于流体力学建立了搅拌摩擦焊接过程热流分析模型,确立了焊接过程中热输入与搅拌头旋转频率、工件运动速度、搅拌头尺寸及材料发生屈服时的剪切应力的关系模型.

(2) 峰值温度约为合金液相线温度的 89%,轴肩产热约占总热量的 87%,搅拌头后部温度高于前部,温度梯度前部大于后部,焊缝前进侧温度梯度小于后退侧.

(3) 轴肩对工件上部材料流动影响较大,下部材料主要受搅拌针影响,搅拌针周围材料粘度的分布范围为 $4.24\times10^{4}\sim5\times10^{6}$ kg/(m·s),与试验结果吻合较好.

参考文献:

[1] 张 华,林三宝,吴 林,等. 搅拌摩擦焊研究进展及前景展望[J]. 焊接学报,2003,24(3):91-96.
Zhang Hua, Lin Sanbao, Wu Lin, *et al*. Current progress and prospect of friction stir welding [J]. Transactions of the China Welding Institution, 2006, 27(11): 81-85.

[2] 栾国红,柴 鹏,孙成斌. 钛合金的搅拌摩擦焊探索[J]. 焊接学报,2005,26(11):83-88.
Luan Guohong, Chai Peng, Sun Chengbin. Preliminary study on friction stir welding of titanium alloy [J]. Transactions of the China Welding Institution, 2005, 26(11): 83-88.

[3] Song M, Kovacevic R. Thermal modelling of friction stir welding in a moving coordinate system and its validation [J]. International Journal of Machine Tools & Manufacture, 2003, 43: 605-615.

[4] Schmidt H, Hattel J. Modelling heat flow around tool probe in friction stir welding [J]. Science and Technology of Welding and Joining, 2005, 10(2): 176-186.

[5] Schmidt H B, Hattel J H. Thermal modeling of friction stir welding [J]. Scripta Materialia, 2008, 58: 332-337.

[6] 李红克,史清宇,赵海燕,等. 热量自适应搅拌摩擦焊热源模型[J]. 焊接学报,2006,27(11):81-85.
Li Hongke, Shi Qingyu, Zhao Haiyan, *et al*. Auo-adapting heat source model for numerical analysis of friction stir welding [J]. Transactions of the China Welding Institution, 2006, 27(11): 81-85.

[7] 赵衍华,林三宝,贺紫秋,等. 2014 铝合金搅拌摩擦焊接过程的数值模拟[J]. 机械工程学报,2006,42(7):92-97.
Zhao Yanhua, Lin Sanbao, He Ziqiu, *et al*. Numerical simulation of 2014 aluminum alloy friction stir welding process [J]. Chinese Journal of Mechanical Engineering, 2006, 42(7): 92-97.

[8] Sheppard T, Jackson A. Constitutive equations for use in prediction of flow stress during extrusion of aluminum alloys [J]. Materials Science and Technology, 1997, 13: 203-209.

[9] Atharifar H, Lin D C, Kovacevic R. Numerical and experimental investigations on the loads carried by the tool during friction stir welding [J]. Journal of Materials Engineering and Performance, 2009, 18(4): 339-350.

作者简介: 冯天涛,男,1979 年出生,讲师,博士研究生. 主要从事搅拌摩擦焊接工艺及其数值模拟的研究. 发表论文 5 篇. Email: fttao79@163.com

通讯作者: 张晓辉,男,教授,博士研究生导师. Email: zhangxh@sdau.edu.cn

Gaussian template is used to smooth the centerline of laser stripe. Secondly, the improved CSS adopts an adaptive K-cosine algorithm, which has a dynamic region of support and excellent noise suppression performance to calculate the curvature of centerline smoothed by large-scale Gaussian template. Thirdly, the local extrema of the curvature extracted by a threshold T are used to candidate feature points. Lastly, the candidate feature points are refined in small-scale Gaussian template. The results showed that the improved CSS algorithm has better robust and anti-interference than the that of CSS algorithm.

Key words: tailored blanks laser welding; structured light; feature point detection; curvature scale space

Effects of shoulder plug depth on joining performance of AA2024/AA2024 friction stir welded joints ZHAO Lei, ZHANG Tiancang, LI Xiaohong, SUN Chengbin (AVIC Beijing Aeronautical Manufacturing Technology Research Institute, Beijing 100024, China). pp 97 – 100

Abstract: By adjusting shoulder plug depth, its effects on joining performance of 3mm thick AA2024/AA2024 friction stir welded joint were studied. The results show that tunnel-type defects exists at the stirring pin advancing side in joint when the shoulder is not pressed. As the shoulder plug depth increases, the tunnel-type defects disappear and oxide defects (commonly known as S line) begin to appear. The number of oxide defects increase firstly and then decreases. S line also appears at the bottom of the weld nugget zone, and becomes gradually longer with shoulder plug depth increasing. The tensile test indicates that the highest tensile strength of AA2024/AA2024 FSW joints is 370 MPa at the welding speed of 100 mm/min, pin rotational speed of 800 r/min and the shoulder plug depth of 0.2 mm, and the highest reduction of area is 3.4%.

Key words: aluminum alloy; friction stirs welding; tensile strength; defect

Effects of shielding gas composition on microstructure and toughness of 440 MPa HSLA steel weld metals with gas metal arc welding XIAO Xiaoming, PENG Yun, MA Chengyong, HE Changhong, TIAN Zhiling (State Key Laboratory of Advanced Steel Processes and Products, Central Iron & Steel Research Institute, Beijing 100081, China). pp 101 – 104

Abstract: The 440 MPa HSLA steel was welded with gas metal arc welding (GMAW), and the microstructure of weld metals and the morphology of inclusions were analyzed with OM, TEM, SEM, and EBSD. The effects of shielding gas on the microstructure, impact toughness of the weld metals and the size, quantity, compositions of inclusions were investigated. The results show that impact toughness of weld metal is bad with 100% CO_2 as shielding gas, and weld metals with good impact toughness can be obtained with 80% Ar + 20% CO_2 and 90% Ar + 10% CO_2 (volume fraction) as shielding gas. The microstructure of weld metal of 100% CO_2 GMAW is made up of ferrite and bainite, and that of both 20% CO_2 GMAW and 10% CO_2 GMAW are predominantly acicular ferrite with small areas of ferrite side plates. With the increasing of the proportion of CO_2 in shielding gas, the amount and dimension of inclusions increase, and the compositions of its main ingredients change. For 440 MPa HSLA steel, welding with proper gas composition can produce welded joints with good properties.

Key words: HSLA; gas metal arc welding; microstructure; toughness; inclusion

Three dimensional model for heat transfer and plastic flow of friction stir welding FENG Tiantao, ZHANG Xiaohui (Shandong Provincial Key Laboratory of Horticultural Machineries and Equipments, Shandong Agriculture University, Taian 271018, China). pp 105 – 108

Abstract: In order to study the temperature field, velocity field and viscosity field of friction stir welding under the interaction of thermal and fluid, the material was regarded as laminar, viscosity, non-Newtonian fluid. Based on the theory of fluid mechanics, three dimensional thermal and fluid model of the friction stir welding was founded. A mathematical relationship between the welding heat input and rotating speed, workpiece motion velocity, size of stirring tool and the shear stress of material was adopted, which is used as the thermal boundary conditions in modeling. Analysis results indicate that the temperature of the head of stirring tool is lower than that of the tail, but the temperature gradient is larger. Affected by material flow around the stirring tool, the temperature in retreating side is higher than that of the advancing side. Velocity and viscosity of upper material is affected mainly by shoulder, while the lower material is affected mainly by stirring pin. The calculated thermal mechanical affected zone (TMAZ) has a good corresponding relationship with the experimental result.

Key words: friction stir welding; fluid mechanics; coupling; shear stress

Analysis of stress concentration factors of overlap joints based on finite element method FU Lei[1], CHENG Ronglong[1], YANG Jianguo[1,2], WANG Tao[1], FANG Hongyuan[1] (1. State Key Laboratory of Advanced Welding and Joining, Harbin Institute of Technology, Harbin 150001, China; 2. Institute of Process Equipment and Control Engineering, Zhejiang University of Technology, Hangzhou 310014, China). pp 109 – 112

Abstract: Stress concentration factors have a significant effect on the load capacity of overlap joint. The influence of joint geometric parameters on stress concentration factors of bilateral welded undermatching overlap joints were studied based on the finite element method, and the stress concentration equation was founded based on regression analysis method. The result shows that the lap length plays the most important role in stress concentration factors. The stress concentration factors at weld root increase with the lap length increasing, weld width decreasing and weld toe smooth transition radius decreasing. The stress concentration factors at weld toe increase with the lap length and weld width increasing. Weld toe with smooth transition radius has little effect on concentration factors at weld toe. The stress concentration equation has a good agreement with the finite element result.

Key words: overlap joint; stress concentration factors; weld root; weld toe; finite element